Statistica Sinica **15**(2005), 407-425

A STATE-SPACE APPROACH TO MODELLING BRAIN DYNAMICS

Moon-Ho Ringo Ho, Hernando Ombao and Robert Shumway

McGill University, University of Illinois at Urbana-Champaign and University of California at Davis

Abstract: We propose a state-space approach for studying the dynamic relationship between multiple brain regions. Our approach decomposes the observed multiple time series into measurement error and the BOLD (blood oxygenation level dependent) signals. The proposed model consists of the activation and connectivity equations. In the activation equation, we model the observed signals at each brain region as a function of the BOLD signal. One special feature of our model for capturing the complexities of the dynamic processes in the brain is that the region-specific time-varying coefficients in the activation equation are subsequently modelled, in the connectivity equation, as a function of the BOLD signals at other brain regions. Because our model has a state-space representation, the parameters are readily estimated by maximum likelihood via a routine application of the Kalman filter and smoother. In this paper, we apply our model to a functional magnetic resonance imaging data set to investigate the attentional control network in the brain.

Key words and phrases: Effective connectivity, functional magnetic resonance imaging, Kalman filter, state-space model.

1. Introduction

Over the last two decades, there has been a dramatic advancement in technology that allows neuroscientists to detect brain signals for studying the complex activities in human brain. In the neuroscience community, there is a growing interest in investigations that target possible interactions between different brain regions. In this paper, we propose a state-space approach for studying the dynamic relationship between multiple brain regions. Our model consists of the activation and connectivity equations which correspond to the observation and state equations in the state-space model framework. In the activation equation, we model the observed signals at each brain region as a function of the BOLD (blood oxygenation level dependent) signal. In the connectivity equation, we model the region-specific time-varying coefficients in the activation equation as a function of the BOLD signal at the other regions. Through a system of two equations, complexities of the dynamic processes in the brain are modelled. Moreover,

the parameters in the model are readily estimated by maximum likelihood via a routine application of the Kalman filter and smoother.

We first give a brief discussion on the functional magnetic resonance imaging (fMRI) data set that we use in this paper. In functional brain imaging studies, the signal changes of interest are caused by neuronal activity, but such electrical activity is not directly detectable by fMRI. The signal being measured in fMRI experiments is called the Blood Oxygenation Level Dependent (BOLD) response, which is a consequence of the hemodynamic changes (including local changes in blood flow, volume and oxygenation level) occurring within a few seconds of changes in neuronal activity. The BOLD signal is usually used as a proxy for the underlying neuronal activity. Most fMRI studies concern the detection of sites of activation ('hot-spots') in the brain and their relationship to the experimental stimulation, and we refer to them as *activation* studies. A typical BOLD response, $x(t)$, usually occurs between 3-10 seconds after the stimulus, $s(t)$, is presented, and reaches its peak at about 6 seconds. The delay of the BOLD response is usually modelled by a hemodynamic response function (HRF), $h(t)$, which weighs the past stimulus values by a convolution

$$x(t) = \int_0^t h(u)s(t-u)\,du, \tag{1.1}$$

where $s(t)$ takes the value '1' when the stimulus is 'ON' and '0' when the stimulus is 'OFF'. The top panel in Figure 1 shows a stimulus presented periodically in a fMRI experiment. The HRF is usually modelled by a Poisson, Gaussian or Gamma density, or by the difference of two Gamma functions. The second panel in Figure 1 shows a typical hemodynamic response function and the bottom panel shows how the BOLD signal looks after convolution with the periodic stimulus function in the top panel. The magnitude of the BOLD signal, denoted as β, varies over brain regions and experimental conditions, and is usually estimated by the general linear model

$$y_i(t) = \alpha_i + \beta_i x_i(t) + e_i(t), \tag{1.2}$$

where $y_i(t)$ is the observed fMRI signal, and $e_i(t)$ is measurement noise at voxel i (voxel is the 3-D generalization of pixel). The coefficient, β_i, measures 'activation' at voxel i in fMRI studies and α_i represents the baseline. Without loss of generality, we assume the fMRI data is detrended here. Detrending is a common pre-processing step in fMRI experiments and attempts to remove the drift (mainly caused by the MRI scanner) present in fMRI data. A priori detrending is not necessary but can simplify the computation. We will comment on how to incorporate a drift component in our approach in the conclusion.

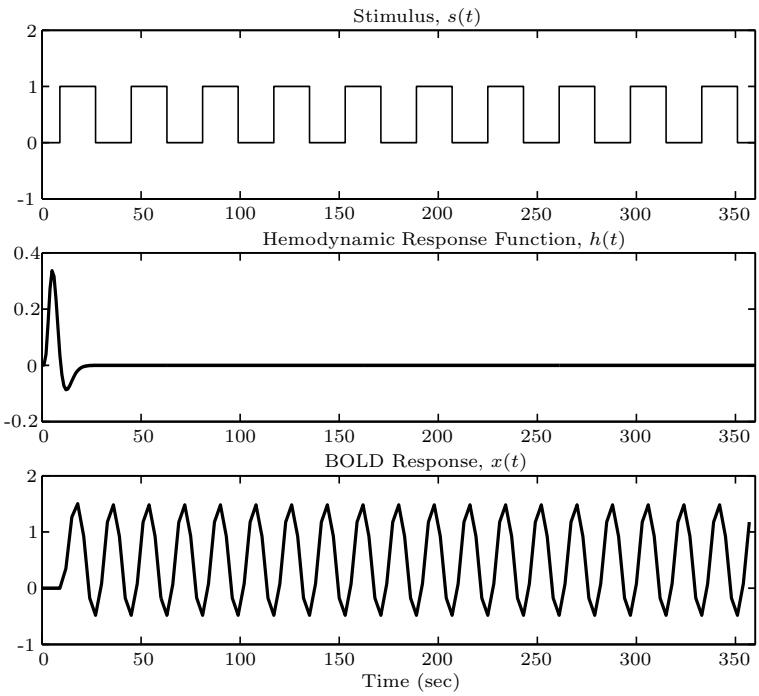

Figure 1. Convolution of hemodynamic response function.

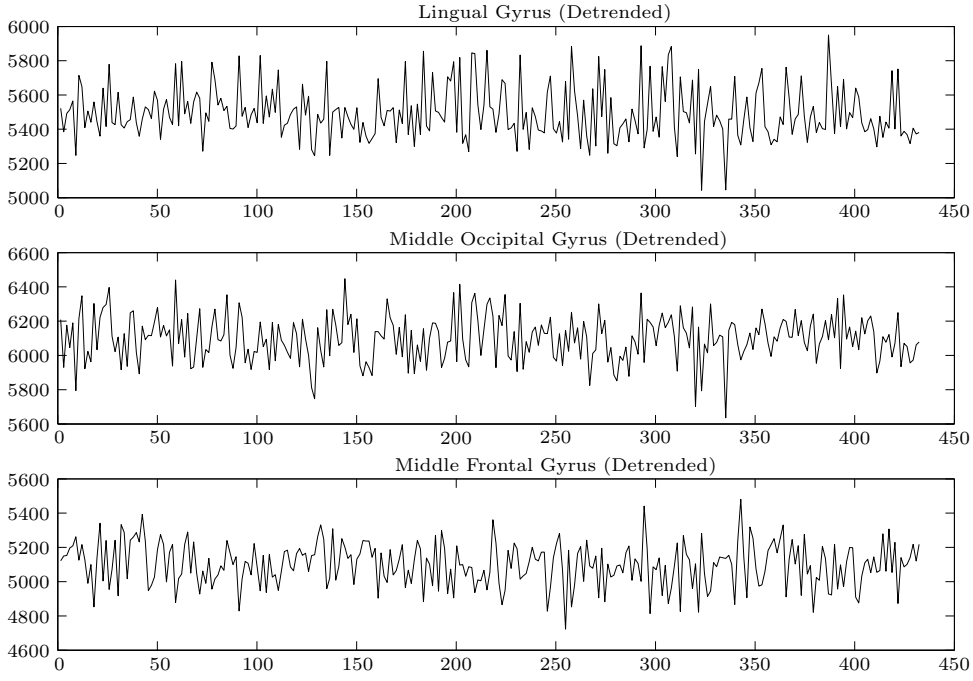

Figure 2. Three detrended fMRI time series.

Figure 2 shows three examples of fMRI time series after they have been detrended by a running-line smoother (Marchini and Ripley (2000)). A running-line smoother is a linear regression fitted to the $k-$nearest neighbors of a given point and used to predict the response at that point. For an fMRI experiment with periodic design (e.g., a block of experimental stimuli and a block of control stimuli are alternatively presented to the subjects), Marchini and Ripley (2000) suggested setting k equal to at least twice the cycle length (one cycle is one block of experimental stimuli plus one block of control stimuli, as in the previous example). These activation studies do not reveal a great deal about how different brain regions relate or 'communicate' with each other. Disparate regions of the brain do not operate in isolation. It is therefore important to characterize the connectivities underlying the fMRI data so as to understand the functional organization of the brain. Influence of one neuronal system on another is referred to as *effective connectivity* (Friston (1994) and Nyberg and McIntosh (2001)). Two common approaches, namely structural equation modelling (see McIntosh and Gonzalez-Lima (1994), for example) and time-varying parameters regression (see Büchel and Friston (1998), for example), have been applied to fMRI data for studying effective connectivity. However, these approaches suffer several limitations. For both approaches, fMRI researchers first choose their regions-of-interest and extract the corresponding time series from the high-dimensional fMRI data of a single subject. In the applications of structural equation modelling, a within-subject covariance matrix of the regions-of-interest is derived and a path analysis model is then fitted to this matrix. Effective connectivity is then measured by the path or structural coefficients. This approach ignores the temporal correlation in the data which can lead to inaccurate standard errors and test statistics. Connectivity between brain regions is also assumed to be time-invariant. Time-varying parameter regression, on the other hand, relaxes this assumption and allows time-varying connectivity. In the applications of time-varying parameter regression, one brain area's time series is regressed on another brain area's time series as

$$y_1(t) = \beta(t) y_2(t) + e(t),$$
$$\beta(t) = \beta(t-1) + w(t),$$

where $e(t)$ and $w(t)$ are independent white noises. The regression coefficient, $\beta(t)$, following a random walk process, measures the dynamic effective connectivity in this approach. Applications of time-varying parameter regression, however, have been limited to studying the relationship between two brain regions so far. A more general way to characterize the dynamics of $\beta(t)$ can be through the functional coefficients model first explored in Chen and Tsay (1993), and later extended to non-linear time series models by Cai, Fan and Yao (2000). Harrison,

Penny and Friston (2000) proposed the use of multivariate/vector autoregressive (MAR) models for modeling effective connectivity. They included interaction term between pairs of regional contemporaneous time series to account for the nonlinear interregional dependence in the models. Lagged regional time series were also included to account for the temporal autocorrelation. Their approach model the brain systems behavior by simply quantifying relationships within the measured data only. Our approach differs from their approach in that we model the brain as a dynamic system so as to understand temporal and spatial order within measured fMRI data. We attempt to account for correlations within the data by invoking state variables whose dynamics generate the data. The MAR approach used by Harrison, Penny and Friston (2000) models temporal effects across different brain regions without using state variables, and inter-regional dependencies within the data were characterized in terms of the historical influence of one region on another. Horwitz(1998) and Horwitz, Tagamets and McIntosh (1999) referred to all the aforementioned approaches as *system-level neural modeling*, which attempts to address the problem that large covariance in inter-regional activity can come about by direct and indirect effects. Recently, Horwitz and his colleagues proposed another approach, referred to as *large-scale neural modelling*, using neurobiologically realistic networks to simulate neural data at multiple spatial and temporal levels, such as single unit electrophysiological data (Deco, Rolls and Horwitz (2004) and Positron Emission Tomography (PET) data (Tagamets and Horwitz (1998)). Their approach is computationally intensive and emphasizes the mimicking of *qualitative* patterns observed in the brain imaging experiments. Statistical estimation of unknown parameters is of secondary importance and these parameters are usually chosen or fixed a priori (usually based on animal studies). The method proposed in this paper can be classified as the system-level neural modeling in Horwitz's terminology. We focus on the state-space modelling approach. Our approach differs primarily in its intent to model the stochastic inter-relationship between the different components of multiple signals. Another important statistical methodology that is related to our work is that of Tiao and Box (1981), who provide very interesting applications to modelling of the relationships between components of a multivariate time series. The distinct feature in our model is a particular form of the dynamic relationship between different brain regions via the connectivity equations (to be defined below).

Our proposed approach can overcome some of the limitations encountered in structural equation modelling and time-varying parameter regression methods. Our method treats the brain as an input-output system. By perturbing the system with known inputs (i.e., experimental stimuli), the measured responses (i.e., observed fMRI signals) are used to estimate various parameters that govern the

evolution of the activation. The proposed method: (1) allows modelling relationships among multiple brain areas; (2) separates out the signal-of-interest (BOLD) from the measurement noise; (3) models the temporal correlation explicitly by the recent history of the experimental inputs. Almost all effective connectivity studies using the two aforementioned methods focus on studying the connectivity from single subject's fMRI data. Inter-subject commonalities and differences in the connectivity pattern are seldom investigated (but see Mechelli, Penny, Price, Gitelman and Friston (2002)). At the end of the paper we discuss how to extend the proposed approach to examine commonalities and differences in the connectivity patterns across subjects or groups of subjects.

2. Effective Connectivity Analysis by State-space Models

In (1.2), the 'activation' β is assumed to be time-invariant, which may not be realistic. Recently some studies reported a 'learning' effect in fMRI experiments, and strong fMRI activation was mainly detected in the beginning of the experiment but weakened overtime (see Milham, Banch, Claus and Cohen (2003), for example). Therefore, it is reasonable to consider activation to be time-varying. Dropping the time-invariant assumption, we can rewrite (1.2) as

$$y_i(t) = \alpha_i + \beta_i(t)x_i(t) + e_i(t).$$

The 'activation' $\beta_i(t)$ is postulated to depend on the BOLD history from itself and/or other brain regions to account for its variation over time. Consider, for example, two regions-of-interest and activation from these two areas as characterized by

$$y_1(t) = \alpha_1 + \beta_1(t)x_1(t) + e_1(t); \tag{2.1}$$
$$y_2(t) = \alpha_2 + \beta_2(t)x_2(t) + e_2(t). \tag{2.2}$$

We refer to (2.1) and (2.2) as the *activation equations*. The 'activation' of both regions-of-interest are allowed to vary over time and the 'activation' from one region is expressed as the BOLD history from itself and another region as follows:

$$\beta_1(t) = \gamma_{1\cdot1}Z_1(t-1) + \gamma_{1\cdot2}Z_2(t-1) + w_1(t), \tag{2.3}$$
$$\beta_2(t) = \gamma_{2\cdot1}Z_1(t-1) + \gamma_{2\cdot2}Z_2(t-1) + w_2(t), \tag{2.4}$$

where $Z_1(t-1) = x_1(t-1)\beta_1(t-1)$ and $Z_2(t-1) = x_2(t-1)\beta_2(t-1)$ represent the BOLD signals from an earlier time point $(t-1)$. We refer to (2.3) and (2.4) as the *connectivity equations*.

Higher order effects of the BOLD history (from $t-2$, $t-3$ and so on) and other covariates of interest (e.g., physiological measures such as respiration

rate and heart beat rate) may also be included in the model. The order of the BOLD history can also vary for different brain regions. Activation may evolve in a nonlinear fashion but we focus on linear functions in this paper. Our formulation considers the brain as a dynamical system which assumes that the instantaneous state of any brain system depends on the history of its input. In this model, effective connectivity is characterized by the coefficients $\gamma_{1\cdot2}$ and $\gamma_{2\cdot1}$ that describe the 'coupling' or 'lead-lag' relationships between the two regions. We can examine hypotheses where (a) there is 'no dynamic coupling' between the two regions ($\gamma_{1\cdot2} = 0$ and $\gamma_{2\cdot1} = 0$); (b) region 2 is a 'leading indicator' of region 1 (e.g., only $\gamma_{1\cdot2} \neq 0$); (c) region 1 is a 'leading indicator' of region 2 (e.g., only $\gamma_{2\cdot1} \neq 0$); (d) a form of 'dynamic coupling' exists between both regions ($\gamma_{1\cdot2} \neq 0$ and $\gamma_{2\cdot1} \neq 0$). It is obvious that if we ignore the connectivity equations and constrain $\beta(t)$ to be invariant over time, we obtain the general linear model used for activation analysis in (1.2).

As pointed out by one of our reviewers, an alternative candidate model for (2.3) and (2.4) is to express the $\beta(t)$ as a function of the history of $\beta(t-1)$, i.e., $\beta_1(t) = \gamma_{1\cdot1}\beta_1(t-1) + \gamma_{1\cdot2}\beta_2(t-1) + w_1(t)$ and $\beta_2(t) = \gamma_{2\cdot1}\beta_1(t-1) + \gamma_{2\cdot2}\beta_2(t-1) + w_2(t)$. We have implemented this alternative but unfortunately the goodness-of-fit and the model prediction based on this alternative model was much worse than our proposed formulation (2.3) and (2.4), at least in the application to the dataset described in Section 4. To save space, we omit the results of this alternative model here. Our proposed approach can be thought of a generalization of this alternative model. We can re-write (2.3) and (2.4) as

$$\begin{aligned}\beta_1(t) &= [\gamma_{1\cdot1}x_1(t-1)]\beta_1(t-1) + [\gamma_{1\cdot2}x_2(t-1)]\beta_2(t-1) + w_1(t),\\ \beta_2(t) &= [\gamma_{2\cdot1}x_1(t-1)]\beta_1(t-1) + [\gamma_{2\cdot2}x_2(t-1)]\beta_2(t-1) + w_2(t),\end{aligned}$$

or, equivalently, as

$$\begin{aligned}\beta_1(t) &= \gamma^*_{1\cdot1}\beta_1(t-1) + \gamma^*_{1\cdot2}\beta_2(t-1) + w_1(t),\\ \beta_2(t) &= \gamma^*_{2\cdot1}\beta_1(t-1) + \gamma^*_{2\cdot2}\beta_2(t-1) + w_2(t),\end{aligned}$$

where $\gamma^*_{i\cdot j}{=}\gamma_{i\cdot j}x_j(t-1)$ for $i = 1, 2$, and $j = 1, 2$. Our model can now be thought of a generalization of the reviewer's alternative but with time-varying 'connectivity', i.e., the magnitude of the connectivity coefficients vary over time in proportional to the historical influence of convoluted hemodynamic response function: $\gamma^*_{i\cdot j}(t) = \gamma_{i\cdot j}x_j(t-1)$. We plan to investigate a general version of time-varying connectivity equations without this proportionality constraint in the future and will report the results in a separate paper.

Our proposed approach integrates activation and effective connectivity analyses into one model. This model can be reformulated as a state-space model (Ho

(2003)). Details will be given in the next section. State-space model provides a unifying framework for describing and modelling a wide class of linear stochastic processes. Classical Box-Jenkins ARIMA models, conditional heteroscedastic models, structural time series models, vector autoregressive moving average models, and many others, can be express as special cases of state-space models (Harvey (1991), Jones (1993) and Shumway and Stoffer (2000)). An advantage of reformulating the current proposed model as a state-space model is that the maximum likelihood estimates for the parameters in (2.1) to (2.4) can be readily computed by routine application of the Kalman filter via prediction error decomposition or the EM (expectation-maximization) algorithm. We consider the latter method in this paper.

3. Parameter Estimation and Statistical Inference

3.1. Maximum likelihood estimation by EM algorithm

A linear Gaussian state-space model is defined as, for $t = 1, \ldots, n$,

$$y_t = \alpha_t + A_t\beta_t + e_t, \quad e_t \sim N_p(0, R_t), \tag{3.1}$$

$$\beta_t = d_t + \Phi_t\beta_{t-1} + w_t, \quad w_t \sim N_k(0, Q_t), \tag{3.2}$$

where y_t is a $p \times 1$ vector of observations and β_t is a $k \times 1$ state vector. The noises, e_t and w_t, are assumed to be independent of each other at all time points and follow Gaussian distribution. The model implies that the development of the system under study, over time, is determined by a series of *'state'* vectors $\beta_1, \ldots, \beta_n$ (they can be observed or unobserved), linearly associated with a series of observations $y_1, \ldots, y_n$. The equation (3.1) is called the observation equation, which has the structure of a linear regression with time varying coefficient vector α_t. Equation (3.2) is called the state equation and describes the dynamics of the states in terms of a Markov (first-order vector autoregressive model) process. The unobserved Markovian process of the states might be of interest in its own right, or as a technical tool for formulating a specific correlation structure. The initial state vector β_0 is assumed to be $N_k(\mu_0, \Sigma_0)$ and independent of the disturbances, e_t and w_t. It is common to set $\mu_0 = 0$ and to assign large values to the diagonal elements of Σ_0 (e.g., $10^6 * I_k$). The classical autoregressive integrated moving average (ARIMA) models can be put into the state-space form, with the latent process of the states containing the lagged observations of the observed process that is not of separate interest. In financial time series analysis, the variance of the observations (i.e., the volatility), which is usually changing over time, can be represented as the latent state. Here, the process of the states measures the stability of a stock market.

The model (2.1) to (2.4) can be reformulated as a state-space model in the form of (3.1) and (3.2):

$$\underbrace{\begin{pmatrix} y_1(t) \\ y_2(t) \end{pmatrix}}_{y_t} = \underbrace{\begin{pmatrix} \alpha_1 \\ \alpha_2 \end{pmatrix}}_{\alpha_t} + \underbrace{\begin{pmatrix} x_1(t) & 0 \\ 0 & x_2(t) \end{pmatrix}}_{A_t} \underbrace{\begin{pmatrix} \beta_1(t) \\ \beta_2(t) \end{pmatrix}}_{\beta_t} + \underbrace{\begin{pmatrix} e_1(t) \\ e_2(t) \end{pmatrix}}_{e_t}, \tag{3.3}$$

$$\underbrace{\begin{pmatrix} \beta_1(t) \\ \beta_2(t) \end{pmatrix}}_{\beta_t} = \underbrace{\begin{pmatrix} \gamma_{1\cdot1}x_1(t-1)\ \gamma_{1\cdot2}x_2(t-1) \\ \gamma_{2\cdot1}x_1(t-1)\ \gamma_{2\cdot2}x_2(t-1) \end{pmatrix}}_{\Phi_t} \underbrace{\begin{pmatrix} \beta_1(t-1) \\ \beta_2(t-1) \end{pmatrix}}_{\beta_{t-1}} + \underbrace{\begin{pmatrix} w_1(t) \\ w_2(t) \end{pmatrix}}_{w_t}, \tag{3.4}$$

$d_t = (0,0)'$, $Q_t = Q$ and $R_t = R$ are diagonal matrices with $(\sigma^2_{w_1}, \sigma^2_{w_2})$ and $(\sigma^2_{e_1}, \sigma^2_{e_2})$ on their diagonals, respectively. For convenience, the unknown parameters in (2.1) to (2.4) are written as $\Theta = (\alpha, \Gamma_v, \Sigma_Q, \Sigma_R)$, where $\alpha = \alpha_t = (\alpha_1, \alpha_2)'$, $\Gamma_v = (\gamma_{1\cdot1}, \gamma_{1\cdot2}, \gamma_{2\cdot1}, \gamma_{2\cdot2})'$, $\Sigma_Q = (\sigma^2_{w_1}, \sigma^2_{w_2})'$, $\Sigma_R = (\sigma^2_{e_1}, \sigma^2_{e_2})'$. As mentioned before, the hemodynamic response function h in (1.1) is chosen a priori by researchers in most fMRI studies, and the A_t are assumed to be known. One can also estimate the parameters in the hemodynamic response function but that involves more complicated computation. The challenge is that these parameters in h usually enter the model nonlinearly. We are currently examining this issue and will discuss it in a separate paper.

The maximum likelihood estimator for the parameter Θ can be obtained using the EM-algorithm of Dempster, Laird and Rubin (1977), as proposed by Shumway and Stoffer (1982). The EM-algorithm requires computation of the Kalman filter and Kalman smoother for β_t. In what follows, we denote the Kalman filter and Kalman smoother estimators for β_t as $\beta_t^{t-1} = E(\beta_t | y_1, \ldots, y_{t-1})$ and $\beta_t^n = E(\beta_t | y_1, \cdots, y_n)$, respectively, with the corresponding mean squared covariance estimator as $P_t^{t-1} = E\{(\beta_t - \beta_t^{t-1}) | y_1, \cdots, y_{t-1}\}$ and $P_t^n = E\{(\beta_t - \beta_t^n) | y_1, \cdots, y_n\}$. The recursion formulae to compute these quantities can be found in many references(see, for example, Anderson and Moore (1979), Jones (1993) and Shumway and Stoffer (2000, Properties P4.1, P4.2, p.313)). Under Gaussian assumptions, we can write the log-likelihood of (3.3) and (3.4) as if the state vectors β_t are observed. Then Shumway and Stoffer (1982) have shown that the log-likelihood can be maximized by following a sequence of expectation and maximization steps given by applying the EM (expectation-maximization) algorithm. Following their results, we developed the following set of recursions to update the unknown parameters Θ:

$$\alpha^{(j)} = \frac{1}{n} \sum_{t=1}^{n} (y_t - A_t \beta_t^n), \tag{3.5}$$

$$\Gamma^{(j)} = \Big(\sum_{t=1}^{n} S_{10,t}A'_{t-1}\Big)\Big(\sum_{t=1}^{n} A_{t-1}S_{00,t}A'_{t-1}\Big)^{-1}, \tag{3.6}$$

$$Q^{(j)} = \frac{1}{n}\sum_{t=1}^{n} (S_{11,t} - \Gamma^{(j-1)}A_{t-1}S'_{10,t} - S_{10,t}A'_{t-1}\Gamma_t^{(j-1)\prime} + \Gamma^{(j-1)}A_{t-1}S_{00,t}A'_{t-1}\Gamma^{(j-1)\prime}), \tag{3.7}$$

$$R^{(j)} = \frac{1}{n}\sum_{t=1}^{n} [(y_t - \alpha^{(j-1)} - A_t\beta_t^n)(y_t - \alpha^{(j-1)} - A_t\beta_t^n)' + A_tP_t^nA'_t], \tag{3.8}$$

where

$$S_{00,t} = \beta_{t-1}^n(\beta_{t-1}^n)' + P_{t-1}^n, \tag{3.9}$$

$$S_{10,t} = \beta_t^n(\beta_{t-1}^n)' + P_{t,t-1}^n, \tag{3.10}$$

$$S_{11,t} = \beta_t^n(\beta_t^n)' + P_t^n. \tag{3.11}$$

Notice that $\Phi_t = \Gamma A_{t-1}$; Γ_v defined earlier is the 'vectorized' version of Γ. The initial mean and covariance cannot be estimated simultaneously, so it is conventional to fix one or both of them.

The overall procedure can be regarded as simply alternating between the Kalman filtering and smoothing recursion and the multivariate normal maximum likelihood estimators, as given by (3.5) to (3.8). Convergence results for the EM-algorithm under general conditions can be found in Wu (1983). We summarize the iterative procedure.

1. Initialize the procedure by selecting starting values for the parameters $\Theta^{(0)}$, and fix μ_0, Σ_0.
   At iteration j $(j = 1, 2, \cdots)$, proceed as follows.
2. Compute the incomplete-data likelihood, $-2\log L(Y_n; \Theta)$ (see, for example, (4.67) in Shumway and Stoffer (2000)).
3. Perform the E-Step. Use Properties (P4.1)−(P4.3) in Shumway and Stoffer (2000, pp.313-321)) to obtain the smoothed values β_t^n, P_t^n and $P_{t,t-1}^n$ for $t = 1, \cdots, n$, using the parameters $\Theta^{(j-1)}$. Use the smoothed values to calculate $S_{11,t}, S_{10,t}, S_{00,t}$ given in (3.9)−(3.11).
4. Perform the M-Step. Update the estimates, α, Γ, Q and R using (3.5)−(3.8), to obtain $\Theta^{(j)}$.
5. Repeat Steps 2−4 to convergence.

3.2. Bootstrap estimation of standard errors

The EM algorithm does not provide an easily computed version of the information matrix, hence it is a challenge to find the variances and covariances of

the estimated parameters. Computation of the information matrix via recursions is possible as in Harvey (1991) or Cavanaugh and Shumway (1986). Versions of the information matrix, obtained from outputs arising naturally in the EM algorithm, such as in Meng and Rubin (1991) or Oakes (1999), are either hard to compute, as in the former case, or involve relatively untractable derivatives, as in the latter. A compromise that is easy to apply and robust toward distributional assumptions is the bootstrap, as derived in Stoffer and Wall (1991). We focus on their methodology here.

Suppose we obtain maximum likelihood estimators for $\Theta = \{\alpha, \Gamma, \Sigma_Q, \Sigma_R\}$ as $\widehat{\Theta} = \{\widehat{\alpha}, \widehat{\Gamma}, \widehat{\Sigma_R}, \widehat{\Sigma_Q}\}$. Define the residuals from these estimators as $\widehat{v}_t = y_t - \widehat{\alpha} - A_t\widehat{\beta}_t^{t-1}$, and construct scaled residuals of the form

$$\widehat{\epsilon}_t = \Sigma_t^{-1/2}\widehat{v}_t, \tag{3.12}$$

where a hat over a quantity indicates that it has been evaluated at the maximum likelihood estimator $\hat{\Theta}$. Then, draw a random sample with replacement from the scaled residuals, say, $\widehat{\epsilon}_t^*, t = 1, \cdots, n$. Rescale the residuals, $v_t^* = \Sigma_t^{1/2}\widehat{\epsilon}_t^*$, to obtain residuals with the correct time-varying covariance matrix. To reconstruct the data, note that

$$y_t^* = \widehat{\alpha} + A_t\widehat{\beta}_t^{t-1} + v_t^* \tag{3.13}$$

and compute the values $\widehat{\beta}_t^{t-1}$, using Property P4.1 and the maximum likelihood estimator Θ with (4.37) in in Shumway and Stoffer (2000) replaced by

$$\widehat{\beta}_t^t = \widehat{\beta}_t^{t-1} + \widehat{K_t}\widehat{v}_t^*. \tag{3.14}$$

Using the reconstructed bootstrap sample to compute maximum likelihood estimators $\Theta^* = \{\alpha^*, \Gamma^*, \Sigma_Q^*, \Sigma_R^*\}$ using the procedure described in Section 3.1. The above bootstrap steps are repeated a large number of times, to obtain $\{\widehat{\Theta}_b^*, b = 1, \cdots, B\}$. The finite sample distribution of $(\widehat{\Theta} - \Theta)$ is approximated by the distribution of $(\widehat{\Theta}_b^* - \widehat{\Theta})$, $b = 1, \cdots, B$. For example, the estimated variance of the estimated parameter $\widehat{\theta}$, can be computed as

$$\hat{\sigma}_{\hat{\theta}}^2 = \frac{1}{B-1}\sum_{b=1}^{B}(\hat{\theta}_b^* - \overline{\theta}^*)^2, \tag{3.15}$$

where $\overline{\theta}^*$ denotes the mean of the bootstrap estimators.

4. Application

In this section, we present an application of the proposed approach for investigating the mechanism of an attentional control network using functional magnetic resonance imaging data from a single subject.

4.1. Attentional control network

Human brain has limited processing capacity, and it is important to have mechanisms to filter out task-irrelevant information and select task-relevant information. Attention is the cognitive function underlying the human brain that can discriminate between relevant and irrelevant information. In a recent review, Frith (2001) argued that there are two types of selection processes in the brain, bottom-up and top-down. Bottom-up selection is driven by the difference between the intrinsic properties of a stimulus. Conversely, top-down selection favors the task-relevant feature(s) of the stimulus, independent of its intrinsic properties. Such top-down selection bias requires coordination of neural activity within the attentional network and is usually referred to as the attentional control. Implementation of the attentional control has been suggested to involve (at least) three systems (e.g., Banich et al. (2000)): (1) a system that involves processing task-relevant stimulus dimension (task-relevant processing system); (2) a system that involves processing task-irrelevant stimulus dimension (task-irrelevant processing system); and (3) a higher order executive control system (source of control) performing the top-down selection bias that may increase the neural activity within the task-relevant processing system and/or may suppress the neural activity within the task-irrelevant processing system. Many studies have found the dorsal lateral prefrontal cortex to be a main source of the attentional control. Depending on the task (visual, auditory, etc.), the sites of the attentional control (task-relevant and task-irrelevant processing systems) might vary.

4.2. Experimental design

There were two phases in the experiment. In the learning phase, the subject learned to associate each of three unfamiliar shapes with a unique color word ('Blue', 'Yellow' and 'Green'), and was to name the three shapes with 100% accuracy before the test phase started. In the test phase, two types of trials were presented. In the *interference* trials, the shape was printed in an ink color incongruent with the color used to name the shape, whereas in the *neutral* trials, the shape was printed in white, which was not a color name for any of the shapes. A block design was used, in which a block of neutral trials was alternated with a block of interference trials. A total of 6 interference and 6 neutral blocks was presented, with each block consisting of 18 trials presented at a rate of one trial every 2 seconds. Each trial consisted of a 300 millisecond fixation cross by a $1,200$ millisecond presentation of the stimulus (shape) and a 500 millisecond inter-trial interval. The subject was instructed to subvocally name each shape

with the corresponding color from the learning phase, while ignoring the ink color in which the shape was presented.

4.3. Data acquisition and pre-processing

A GE Signa (1.5 T) magnetic resonance imaging system equipped for echo-planar imaging (EPI) was used for data acquisition. For each run, a total of 300 EPI images was acquired (TR=1,517 ms, TE = 40 ms, flip angle= 90^o), each consisting of 15 contiguous slices (thickness = 7 mm, in-plan resolution = 3.75 mm, parallel to the AC-PC line). A high resolution 3D anatomical set (T1-weighted 3-dimensional spoiled gradient echo images) was also collected. The head coil was fitted with a bite bar to minimize head motion during the session. Stimuli were presented on a goggle system. Interested readers can find more details about the experiment in Milham, Banich, Claus, and Cohen (2003). The first seven volumes of the images were discarded to allow the MR signal to reach steady state.

4.4. Identification of region of interests

For illustration, three regions were selected to investigate the attentional control in the Stroop task. They were the lingual gyrus, the middle occipital gyrus, and the dorsolateral prefrontal cortex. The lingual gyrus (LG) is a visual area sensitive to color information (Corbetta et al. (1991)) representing a *site for processing task-irrelevant information* (i.e., the ink color) in the present experiment (Kelley et al. (1998)). The middle occipital gyrus (MOG) is another visual area sensitive to shape information and represents *a site for processing task-relevant information* (the shape's form). The dorsolateral prefrontal cortex (DLPFC) is selected to represent the *source of attentional control*. These areas were also found to be significantly activated in the interference trials compared to neutral trials in this experiment (see Milham et al. (2003)).

4.5. Statistical analysis

The time series of the three selected ROIs are shown in Figure 2. The conceptual model for attentional control network is tested by the state-space approach described in the previous section. We use $y_1(t), y_2(t)$ and $y_3(t)$ to denote the detrended fMRI time series from LG, MOG and DLPFC respectively. Various possible mechanisms of the attentional control network were explored: whether DLPFC suppresses the activation of LG, facilitates the activation of MOG, or both; if there is reciprocal suppression between LG and MOG (as our brain's processing capacity is limited, the LG and MOG may need to compete for the 'resources'); whether there is feedback from LG and MOG on DLPFC. We

present below the state-space formulation of our proposed model which allows LG, MOG and DLPFC to influence each other directly.

Observation Equation

$$\begin{pmatrix} y_1(t) \\ y_2(t) \\ y_3(t) \end{pmatrix} = \begin{pmatrix} \alpha_1 \\ \alpha_2 \\ \alpha_3 \end{pmatrix} + \begin{pmatrix} x_1(t) & 0 & 0 \\ 0 & x_2(t) & 0 \\ 0 & 0 & x_3(t) \end{pmatrix} \begin{pmatrix} \beta_1(t) \\ \beta_2(t) \\ \beta_3(t) \end{pmatrix} + \begin{pmatrix} e_1(t) \\ e_2(t) \\ e_3(t) \end{pmatrix}.$$

State Equation

$$\begin{pmatrix} \beta_1(t) \\ \beta_2(t) \\ \beta_3(t) \end{pmatrix} = \begin{pmatrix} \gamma_{1\cdot1}x_1(t-1) & \gamma_{1\cdot2}x_2(t-1) & \gamma_{1\cdot3}x_3(t-1) \\ \gamma_{2\cdot1}x_1(t-1) & \gamma_{2\cdot2}x_2(t-1) & \gamma_{2\cdot3}x_3(t-1) \\ \gamma_{3\cdot1}x_1(t-1) & \gamma_{3\cdot2}x_2(t-1) & \gamma_{3\cdot3}x_3(t-1) \end{pmatrix} \begin{pmatrix} \beta_1(t-1) \\ \beta_2(t-1) \\ \beta_3(t-1) \end{pmatrix} + \begin{pmatrix} w_1(t) \\ w_2(t) \\ w_3(t) \end{pmatrix}.$$

This model was fitted by using the EM-algorithm described in the previous section.

Table 1. Model fitting summary.

Model	Γ	$-2*$Log-Likelihood	Number of Parameters	BIC
M1	$\begin{pmatrix} \gamma_{1\cdot1} & \gamma_{1\cdot2} & \gamma_{1\cdot3} \\ \gamma_{2\cdot1} & \gamma_{2\cdot2} & \gamma_{2\cdot3} \\ \gamma_{3\cdot1} & \gamma_{3\cdot2} & \gamma_{3\cdot3} \end{pmatrix}$	9129.1	36	32.37
M2	$\begin{pmatrix} \gamma_{1\cdot1} & 0 & \gamma_{1\cdot3} \\ 0 & \gamma_{2\cdot2} & \gamma_{2\cdot3} \\ \gamma_{3\cdot1} & \gamma_{3\cdot2} & \gamma_{3\cdot3} \end{pmatrix}$	9130.2	34	32.35
M3	$\begin{pmatrix} \gamma_{1\cdot1} & 0 & \gamma_{1\cdot3} \\ 0 & \gamma_{2\cdot2} & \gamma_{2\cdot3} \\ 0 & 0 & \gamma_{3\cdot3} \end{pmatrix}$	9262.7	32	32.80
M4	$\begin{pmatrix} \gamma_{1\cdot1} & \gamma_{1\cdot2} & 0 \\ \gamma_{2\cdot1} & \gamma_{2\cdot2} & 0 \\ 0 & 0 & \gamma_{3\cdot3} \end{pmatrix}$	9241.3	32	32.73
M5	$\begin{pmatrix} \gamma_{1\cdot1} & 0 & 0 \\ 0 & \gamma_{2\cdot2} & 0 \\ \gamma_{3\cdot1} & \gamma_{3\cdot2} & \gamma_{3\cdot3} \end{pmatrix}$	9276.3	32	32.85
M6	$\begin{pmatrix} \gamma_{1\cdot1} & 0 & 0 \\ 0 & \gamma_{2\cdot2} & 0 \\ 0 & 0 & \gamma_{3\cdot3} \end{pmatrix}$	9276.4	30	32.83

4.6. Results

A total of six models were fitted and the fit summary is shown in Table 1. We report $-2*$Log-Likelihood and BIC (Bayesian Information Criterion) for model comparison purposes. For those models with nested relationships, we

perform a likelihood-ratio test (LRT) to check if the model can be simplified. The results are summarized in Table 2. From both the nested model comparisons and BIC, among the six candidate models, M2 fits the best in terms of goodness-of-fit and model parsimony. We also checked the normality and homoscedasticity assumptions based on the residuals. No significant violation of assumptions were found and we therefore skip the details here. The maximum likelihood estimates and the standard errors computed by the bootstrap (250 bootstrapped samples) are shown in Table 3.

Table 2. Model comparison summary.

Model Comparisons	LRT	degree of freedom	p-value
M1 vs. M2	1.1	2	0.42
M1 vs. M4	112.2	4	$< .0001$
M2 vs. M3	132.5	2	$< .0001$
M2 vs. M5	146.1	2	$< .0001$

From Table 3, we can see that there is a significant suppression from DLPFC on LG ($\gamma_{1\cdot3}$), and a relatively weaker facilitation from DLPFC on MOG ($\gamma_{2\cdot3}$). These results are consistent with the proposal of Banich et al (2000). We, also find that there is positive feedback from the LG and MOG on DLPFC ($\gamma_{3\cdot1}$ and $\gamma_{3\cdot2}$). Moreover, DLPFC shows negative self-feedback control on itself ($\gamma_{3\cdot3}$). Our results provide support for the implementation of an attentional control network. The present result is based on a single subject. More fMRI data will be analyzed in the future to cross-validate this result.

Table 3. Maximum Likelihood Estimators and Standard Errors for M2.

Parameters	Maximum Likelihood Estimators	Standard Errors
$\begin{pmatrix}\alpha_1\\ \alpha_2\\ \alpha_3\end{pmatrix}$	$\begin{pmatrix}-1.58\\ -1.01\\ -2.19\end{pmatrix}$	$\begin{pmatrix}10.05\\ 8.47\\ 7.37\end{pmatrix}$
$\begin{pmatrix}\gamma_{1\cdot1} & 0 & \gamma_{1\cdot3}\\ 0 & \gamma_{2\cdot2} & \gamma_{2\cdot3}\\ \gamma_{3\cdot1} & \gamma_{3\cdot2} & \gamma_{3\cdot3}\end{pmatrix}$	$\begin{pmatrix}2.19 & -- & -6.31\\ -- & 1.88 & 5.71\\ 2.69 & 0.62 & -2.01\end{pmatrix}$	$\begin{pmatrix}0.04 & -- & 0.25\\ -- & 0.01 & 0.01\\ 1.24 & 0.13 & 0.35\end{pmatrix}$
$\begin{pmatrix}\sigma^2_{w1}\\ \sigma^2_{w2}\\ \sigma^2_{w3}\end{pmatrix}$	$\begin{pmatrix}8.67\\ 0.55\\ 36.34\end{pmatrix}$	$\begin{pmatrix}1.47\\ 0.14\\ 12.57\end{pmatrix}$
$\begin{pmatrix}\sigma^2_{e1}\\ \sigma^2_{e2}\\ \sigma^2_{e3}\end{pmatrix}$	$\begin{pmatrix}2122.3\\ 1475.0\\ 1608.4\end{pmatrix}$	$\begin{pmatrix}385.36\\ 300.50\\ 167.18\end{pmatrix}$

5. Conclusion

Incorporating Drift

For convenience, we detrended the data first before fitting our model. A priori detrending is not a necessary step and the drift component can be incorporated in our model. For illustration, we assume the drift component follows a simple random walk process in (2.1) and (2.2) as

$$\begin{aligned} y_1(t) &= \alpha_1(t) + \beta_1(t)x_1(t) + e_1(t), \\ y_2(t) &= \alpha_2(t) + \beta_2(t)x_2(t) + e_2(t), \\ \alpha_1(t) &= \alpha_1(t-1) + \varepsilon_1(t), \\ \alpha_2(t) &= \alpha_2(t-1) + \varepsilon_2(t). \end{aligned}$$

We can express the above, (2.3) and (2.4), in state-space form as

$$\underbrace{\begin{pmatrix} y_1(t) \\ y_2(t) \end{pmatrix}}_{y_t} = \underbrace{\begin{pmatrix} x_1(t) & 0 & 1 & 0 \\ 0 & x_2(t) & 0 & 1 \end{pmatrix}}_{A_t} \underbrace{\begin{pmatrix} \beta_1(t) \\ \beta_2(t) \\ \alpha_1(t) \\ \alpha_2(t) \end{pmatrix}}_{\beta_t} + \underbrace{\begin{pmatrix} e_1(t) \\ e_2(t) \end{pmatrix}}_{e_t},$$

$$\underbrace{\begin{pmatrix} \beta_1(t) \\ \beta_2(t) \\ \alpha_1(t) \\ \alpha_2(t) \end{pmatrix}}_{\beta_t} = \underbrace{\begin{pmatrix} \gamma_{1\cdot1}x_1(t-1) & \gamma_{1\cdot2}x_2(t-1) & 0 & 0 \\ \gamma_{2\cdot1}x_1(t-1) & \gamma_{2\cdot2}x_2(t-1) & 0 & 0 \\ 0 & 0 & 1 & 0 \\ 0 & 0 & 0 & 1 \end{pmatrix}}_{\Phi_t} \underbrace{\begin{pmatrix} \beta_1(t-1) \\ \beta_2(t-1) \\ \alpha_1(t-1) \\ \alpha_2(t-1) \end{pmatrix}}_{\beta_{t-1}} + \underbrace{\begin{pmatrix} w_1(t) \\ w_2(t) \\ \varepsilon_1(t) \\ \varepsilon_2(t) \end{pmatrix}}_{w_t}.$$

Other forms of drift, such as a stochastic cubic spline, can be put in the state-space form in a similar way.

Time-varying Connectivity

In the present formulation of the state-space model, connectivity between brain areas ($\gamma_{i\cdot j}$s) is assumed to be time-invariant. This may not be true in general. There is increasing evidence that the connectivity between brain areas is dynamic, i.e., it is varying over the experimental context and time (e.g., McIntosh and Gonzalez-Lima (1994) and Büchel and Friston (1998)). We are currently developing an approach to modelling the dynamic characteristics of the connectivity by using a moving window method. We assume the process within this window is locally stationary (i.e., the connectivity is constant within this window). The

model (2.1)−(2.4) is fitted to the time series data within this 'window', which is then shifted forward by some amount and the model refitted using the data within the new window. As a result, a trajectory of the connectivity coefficient can be obtained which can provide some insight on how the effective connectivity evolves over time.

Multiple subjects analysis

In this paper, we focused the analysis on fMRI data from a single-subject. In fMRI experiments, data are usually collected from multiple subjects. Estimates for connectivity can vary greatly across subjects. This raises the question of whether these differences in connectivity are significant or simply due to chance. Therefore, it is important to develop a method to characterize subject-specific variability in connectivity that permits evaluation of between-subject or between-group differences. We are working on two possible approaches. The first is a meta-analytic two-stage approach. The first stage is to analyze each subject's data separately. Then we combine information across subjects in the second stage by combining hypothesis tests (i.e., significance of the connectivity parameter estimates) or combining estimates of treatment effects (i.e., estimates of the connectivity parameters). The second approach is to simultaneously analyze multi-subject fMRI data in a single stage to accommodate subject-specific variations in connectivity. The proposed model (2.1)−(2.4) has a state-space representation for single subject data. It can be shown that this representation can be preserved in a model with multiple subject's data simultaneously analyzed. The results of this research will be reported in a separate paper.

Final Remarks

In this paper, we gave an application to data from a block design fMRI experiment. The proposed approach can handle fMRI data collected from an event related design as well. Each event's effect can be characterized by its own $\beta(t)$ in the activation and the state equations. In principle, there is no limitation on the number of regions one can study (as long as the model is identified). Practically, however, if there are a large number of regions involved, a large number of parameters are required to be estimated. Fast and efficient optimization algorithms still need to be developed to handle such situations.

Acknowledgement

We thank Mike Milham for the permission to use, and the help in preparation of, the fMRI data used in this paper. M-H. Ho and H. Ombao thank George Tiao for helpful discussions during his visit to UIUC in the Fall of 2002. This research was funded in part by the National Sciences and Engineering Council of Canada Grants 298244 to the first author, National Science Foundation Grants DMS

0102511 and 0405243 to the second author. We thank the Editor, an associate editor, and two anonymous reviewers for their helpful comments on this paper.

Correspondence concerning this article should be addressed to Moon-Ho Ringo Ho, Department of Psychology, McGill University, Montreal, Quebec, Canada H3A 1B1.

References

Anderson, B. D. O. and Moore, J. B. (1979). *Optimal Filtering*. Prentice-Hall, Englewood Cliffs.

Banich, M. T., Milham, M. P., Atchley, R., Cohen, N. J., Webb, A., Wszalek, T., Kramer, A. F., Liang, Z. P., Wright, A., Shenker, J. and Magin, R. (2000). fMRI studies of stroop tasks reveal unique roles of anterior and posterior brain systems in attentional selection. *J. Cognitive Neuroscience* **12**, 988-1000.

Büchel, C. and Friston, K. (1998). Dynamic changes in effective connectivity characterized by variable parameter regression and Kalman filtering. *Human Brain Mapping* **6**, 403-408.

Cai, Z., Fan, J. and Yao, Q. (2000). Functional coefficient regression models for non-linear time series. *J. Amer. Statist. Assoc.* **95**, 941-956.

Chen, R. and Tsay, R. (1993). Functional coefficient autoregressive models. *J. Amer. Statist. Assoc.* **88**, 298-308.

Cavanaugh, J. E. and Shumway, R. H. (1986). On computing the expected Fisher information matrix for state-space model parameters. *Statist. Probab. Lett.* **26**, 347-355.

Corbetta, M., Miezin, F. M., Dobmeyer, S., Shulman, G. L. and Petersen, S. E. (1991). Selective and divided attention during visual discriminations of shape, color, and speed: functional anatomy by positron emission tomography. *J. Neuroscience* **8**, 2383-2402.

Dempster, A., Laird, N. and Rubin, D. (1977). Maximum likelihood from incomplete data via the EM algorithm. *J. Roy. Statist. Soc. Ser. B* **39**, 1-38.

Deco, G., Rolls, E. T. and Horwitz, B. (2004). Integrating fMRI and single-cell data of visual working memory. *Neurocomputing* **58-60**, 729-737.

Friston, K. (1994). Functional and effective connectivity in neuroimaging: a synthesis. *Human Brain Mapping* **2**, 56-78.

Frith, C. (2001). A framework for studying the neural basis of attention. *Neuropsychologia* **39**, 1367-1371.

Harrison, L., Penny, W. D. and Friston, K. (2003). Multivariate autoregressive modeling of fMRI time series. *Neuroimage* **19**, 1477-1491.

Harvey, A. C. (1989). *Forecasting, Structural Time Series Models and the Kalman Filter*. Cambridge University Press, Cambridge.

Ho, M. R. (2003). *Modelling effective connectivity in functional magnetic resonance imaging data by state-space models. Unpublished doctoral dissertation*, University of Illinois at Urbana-Champaign.

Horwitz, B. (1998). Using functional brain imaging to understand human cognition. *Complexity* **3**, 39-52.

Horwitz, B., Tagamets, M. and McIntosh, A. R. (1999). Neural modeling, functional, brain imaging, and cognition. *Trends in Cognitive Sciences* **3**, 91-98.

Jones, R. H. (1993). *Longitudinal Data with Serial Correlation: A State Space Approach*. Chapman and Hall, London.

Kelley, W. M., Miezin, F. M., McDermott, K. B., Buckner, R. L., Raichle, M. E., Cohen, N. J., Ollinger, J. M., Akbudak, E., Conturo, T. E., Snyder, A. Z. and Petersen, S. E. (1998).

Hemispheric specialization in human dorsal frontal cortex and medial temporal lobe for verbal and nonverbal memory encoding. *Neuron* **20**, 927-936.

Marchini, J. L. and Ripley, B. D. (2000). A new statistical approach to detecting significant activation in functional MRI. *Neuroimage* **12**, 366-380.

McIntosh, A. R. and Gonzalez-Lima, F. (1994). Structural equation modeling and its application to network analysis of functional brain imaging. *Human Brain Mapping* **2**, 2-22.

Mechelli, A., Penny, W., Price, C., Gitelman, D. and Friston, K. J. (2002). Effective connectivity and inter-subject variability: using a multi-subject network to test differences and commonalities. *Neuroimage* **17**, 1459-1469.

Meng, X. L. and Rubin, D. B. (1991). Using EM to obtain asymptotic variance-covariance matrices: The SEM algorithm. *J. Amer. Statist. Assoc.* **86**, 899-909.

Milham, M.P., Banich, M., Claus, E. and Cohen, N. (2003). Practice-related effects demonstrate complementary role of anterior cingulate and prefrontal cortices in attentional control. *Neuroimage* **18**, 483-493.

Nyberg, L. and McIntosh, A. R. (2001). Functional neuroimaging: network analysis. In *Handbook of Functional Neuroimaging of Cognition*, (Edited by R. Cabeza and A. Kingstone), 49-72. MIT Press, Cambridge.

Oakes, D. (1999). Direct calculation of the information matrix via the EM algorithm. *J. Roy. Statist. Soc. Ser. B* **61**, 479-482.

Shumway, R. H. and Stoffer, D. S. (2000). *Time series analysis and its applications*. Springer, New York.

Stoffer, D. S. and Wall, K. (1991). Bootstrapping state-space models: Gaussian maximum likelihood estimation and the Kalman filter. *J. Amer. Statist. Assoc.* **86**, 1024-1033.

Tagamets, M. A. and Horwitz, B. (1998). Integrating electrophysiological and anatomical experimental data to create a large-scale model that simulates a delayed match-to-sample human brain imaging study. *Cerebral Cortex* **8**, 310-320.

Tiao, G. and Box, G. (1981). Modelling multiple time series with applications. *J. Amer. Statist. Assoc.* **76**, 802-816.

Wu, C. F. (1983). On the convergence properties of the EM algorithm. *Ann. Statist.* **11**, 95-103.

Department of Psychology, McGill University 1205, Dr. Penfield Avenue, Montreal, Quebec, H3A1B1, Canada.

E-mail: mho@ego.psych.mcgill.ca

Department of Statistics, University of Illinois, 104-A Ilhni Hall, 725 S. Wright St., Champaign, IL 61820, U.S.A.

E-mail: ombao@uiuc.edu

Department of Statistics, University of California, Davis, 360 Kerr Hall, one Shields Ave., Davis, CA 95616, U.S.A.

E-mail: rhshumway@ucdavis.edu

(Received November 2003; accepted December 2004)